Pramana – J Phys. (2022) 96:171
https://doi.org/10.1007/s12043-022-02407-x

Theoretical investigation of magnesium compositional variation of structural and optoelectronic properties of wurtzite $Mg_xZn_{1-x}Se$ ternary alloys through first-principle calculations

UTPAL SARKAR[1,2], MANISH DEBBARMA[1], DEBANKITA GHOSH[1] and SURYA CHATTOPADHYAYA[1,*]

[1]Department of Physics, Tripura University, Suryamaninagar 799 022, India
[2]Department of Physics, Government Degree College, Kamalpur 799 285, India
*Corresponding author. E-mail: surya_ju@yahoo.com

MS received 16 December 2021; revised 14 March 2022; accepted 4 April 2022

Abstract. First-principle calculations are carried out to explore magnesium composition-dependent structural and optoelectronic features of wurtzite $Mg_xZn_{1-x}Se$ ternary alloys. Analyses show a nearly linear enhancement in lattice constants (a_0, c_0) but a reasonably nonlinear reduction in bulk modulus (B_0) with increasing Mg composition. Successive incorporation of Mg atom(s) in place of Zn in the w-ZnSe crystal results in three direct-band gap (Γ–Γ) semiconductor ternary alloys. The fundamental band gap shows fairly nonlinear enhancement with increasing Mg composition. Each of the considered wurtzite specimens is optically anisotropic. The computed components of the refractive index give uniaxial birefringence. Peaks in the dielectric function spectrum of all the specimens in the ultraviolet (UV) region are contributed exclusively or collectively by Se-4p to Mg-4s, 3p and Zn-5s, 4p electronic excitations. With the enhancement in the fundamental band gap, static optical constants $\varepsilon_1(0)$, $n(0)$ and $R(0)$ of the specimens reduce, while critical point energy in their $\varepsilon_2(\omega)$, $k(\omega)$, $\sigma(\omega)$, $\alpha(\omega)$ spectra enhances.

Keywords. Wurtzite MgZnSe ternary alloys; modified Becke–Johnson-generalised gradient approximation; structural properties; optoelectronic features; optical anisotropy; birefringence.

PACS Nos 45.10.Ab; 62.20.Dc; 62.20.Dx; 62.20.de; 81.40.Jj

1. Introduction

In recent years, the requirement for semiconductor materials in material science and engineering is tremendously increasing to meet their demands in fabricating various optoelectronic devices for specific applications. On many occasions, such fabrication processes are disrupted due to the unavailability of semiconductors with compatible optoelectronic properties. The problem can be resolved by manipulating the optoelectronic properties of some basic semiconductors of known properties by synthesising their semiconductor alloys. Such semiconductor alloys may possess compatible optoelectronic properties required to fabricate that specific optoelectronic device. The synthesis of ternary alloys is the preliminary initiative in this regard. The objectives of the present study are to amalgamate wurtzite (B4) zinc selenide (ZnSe) and magnesium selenide (MgSe) having dissimilar band gaps and optoelectronic features to simulate a set of three wurtzite $Mg_xZn_{1-x}Se$ ($0 \leq x \leq 1$) ternary alloys and to calculate their structural, electronic and optical properties.

Experimental investigations have confirmed that ZnSe [1] and MgSe [2] can exist in wurtzite (B4) structure. Both w-ZnSe and w-MgSe are wide-direct (Γ–Γ) fundamental band-gap semiconductors [1,3]. Yim and Stofko [4] conducted experimental observations on vapour-phase epitaxial growth of a single-crystal layer of ZnSe on GaAs, GaP and sapphire substrates. Park and Chan have investigated photoconductivity spectral responses and lattice constants of hexagonal ZnSe [5]. Zhang *et al* have investigated zinc-blende to wurtzite

Electronic supplementary material: The online version of this article (https://doi.org/10.1007/s12043-022-02407-x) contains supplementary material, which is available to authorized users

Published online: 08 September 2022

phase transformation of ZnSe films using pulsed laser deposition technique [6]. Wang *et al* have prepared w-ZnSe nanoparticles from zb-ZnSe single crystal with femtosecond pulsed laser ablation technique [7]. Lattice constants (a, c), internal cell parameter (u) and the c/a ratio of w-ZnSe were measured in a couple of experiments [1,4]. Atroshchenko *et al* have performed an experiment to see the effects of doping of tellurium on the structural properties of w-ZnSe [8]. From several first-principle investigations, we have also received information regarding the stability and lattice parameters of w-MgSe and w-ZnSe [9], structural stability, high-pressure phases, structural properties of w-MgSe [3,9–15], wurtzite-to-rock-salt structural phase transitions in MgSe [13], band structure and electronic properties of w-MgSe [3,10,11,14], phase stability, lattice dynamics and thermodynamic properties of w-MgSe [16], phase stability and electronic structure of w-MgSe [17], structural properties of w-ZnSe [18], electronic properties of w-ZnSe [20–23] and optical properties of w-ZnSe [23]. Momida and Oguchi have theoretically investigated the effects of lattice parameters on the piezoelectric features of w-ZnSe [24].

The literature mentioned earlier reveals that the wurtzite ZnSe and MgSe have attractive and distinguished optoelectronic features. Therefore, their amalgamation by incorporating Mg atoms in the w-ZnSe unit cell at different compositions will result in a set of wurtzite $Mg_xZn_{1-x}Se$ ternary alloys. This paper contains the calculated structural, electronic and optical features of the wurtzite specimens within this ternary system for magnesium compositions $x = 0.0, 0.25, 0.50, 0.75, 1.0$ with reliable exchange-correlation (XC) potentials. The magnesium concentration (x) dependence of these properties is also reported in this paper. Any experimental investigation or theoretical calculations regarding the features of these ternary alloys mentioned earlier has not yet been reported. Hence, we cannot compare any calculated properties in the present paper.

2. Computational details

We have performed our calculations by using density functional theory [25,26] based full-potential linearised augmented plane-wave (FP-LAPW) approach [27]. It is practically used through WIEN2K [28], which is an efficient code for computing various properties of crystalline compounds. Exchange-correlation (XC) potentials for structural and optoelectronic properties are computed with Wu–Cohen-generalised gradient approximation (WC-GGA) [29] and modified Becke–Johnson (mBJ)-GGA scheme [30], respectively.

The FP-LAPW approach considers that atoms of the compound are located inside the spheres of a muffin-tin (MT) structure. The wave function inside MT-spheres is expressed in spherical harmonics with the maximum value of angular momentum $l_{max} = 10$. The same in the interstitial region is expressed on the plane-wave basis with maximum vector in charge density Fourier expansion as $G_{max} = 16\ (\text{a.u.})^{-1}$ and $K_{max} = 8.0/R_{MT}$ as the maximum cut-off wave vector. The selected MT-sphere radius containing zinc, magnesium and selenium atoms as 2.12, 2.12 and 2.02 a.u., respectively, confirms non-overlapping atomic spheres and prevents any charge leakage from MT-sphere. A $10 \times 10 \times 10$ optimised k-mesh is included in the calculation and selected from a variation of total energy with the number of k-points. The core-valence separation is ensured by selecting -6.0 Ry as the core cut-off energy. The valence electrons are treated with scalar relativistic approximation, while core electrons are treated with a fully relativistic approximation. The self-consistent field (SCF) approximation is employed to achieve convergence in total energy. In these calculations, iterations are terminated when the energy difference between two consecutive steps is less than 10^{-5} Ry.

Initially, we designed $2 \times 2 \times 1$ cells for w-ZnSe (space group: P63mc) with 16 atoms with their experimentally measured lattice constants [4]. The $2 \times 2 \times 1$ cells for w-$Mg_xZn_{1-x}Se$ ternary specimens and the terminal binary w-MgSe have been simulated by repeated incorporation of magnesium atom(s) in the place of zinc atom(s) in the binary w-ZnSe unit cell. The crystal structures are visualised with the XCrySDen graphic code [31]. The hexagonal wurtzite crystal structures for ZnSe, $Mg_{0.25}Zn_{0.75}Se$, $Mg_{0.50}Zn_{0.50}Se$, $Mg_{0.75}Zn_{0.25}Se$ and MgSe are presented as figures SF1a–e, respectively, in the Supplementary Materials.

3. Results and discussions

3.1 *Structural properties*

For each specimen under the w-$Mg_xZn_{1-x}Se$ system, we have varied the total energy (E) with the unit cell volume (V), keeping the c/a ratio fixed. With Murnaghan's equation of state [32], the resultant parabolic E–V curve is then fitted to obtain minimum energy (E_0), equilibrium volume (V_0), bulk modulus (B_0) and internal parameter u for the considered crystal. Subsequently, we have varied the total energy of the cell with its c/a ratio keeping its volume fixed at V_0. From the computed value of c/a at minimum energy, we have calculated the equilibrium lattice constants (a_0, c_0) of the wurtzite unit

Table 1. Calculated values of a_0, c_0, c_0/a_0, u, B_0 and E_g.

Compound	a_0 (Å)	c_0 (Å)	c_0/a_0	u	B_0 (GPa)	E_g (Γ–Γ) (eV)
ZnSe	3.993	6.534	1.6363	0.375	65.88	2.843
	4.003[a*], 3.974[b*], 4.00[c*]	6.540[a*], 6.506[b*], 6.52[c*]	1.634[d*]	0.375[e*]		2.87[f*]
	4.008[a], 4.043[b] 4.07[c], 3.974[d], 4.05[e]	6.609[a], 6.703[b], 6.69[c], 6.506[d], 6.64[e]	1.642[c], 1.637[d], 1.642[e]	0.371[b,h] 0.375[c,d] 0.374[e]	65.9[a], 63.30[c]	1.43[f1], 2.75[f2], 2.2[g], 1.07[h1], 1.327[h2]
$Mg_{0.25}Zn_{0.75}Se$	4.046	6.609	1.6335	0.375	59.91	3.072
$Mg_{0.50}Zn_{0.50}Se$	4.096	6.682	1.6313	0.375	55.21	3.294
$Mg_{0.75}Zn_{0.25}Se$	4.149	6.755	1.6281	0.375	50.68	3.616
MgSe	4.200	6.822	1.6243	0.375	46.44	4.173
	4.145[g*]		1.622[g*]			
	4.144[a], 4.237[i] 4.319[j], 4.079[k] 4.165[l1], 4.235[l2] 4.251[m], 4.196[n] 4.19[o1], 4.28[o2] 4.163[p1], 4.252[p2]	6.809[a], 6.837[i] 6.799[l1], 6.979[l2] 6.889[m], 6.825[n] 6.64[o1], 6.76[o2] 6.753[p1], 6.896[p2]	1.614[i] 1.602[j] 1.628[k] 1.620[m] 1.587[o1] 1.578[o2]	0.379[i] 0.38[j] 0.376[k] 0.377[m] 0.377[n] 0.377[p1,p2]	48.2[a], 50[i], 56[j] 52.2[l1], 50.8[l2] 45.08[m], 50[n] 49.3[o1], 43.9[o2] 50.8[p1], 44.4[p]	2.206[i], 2.310[m1], 4.227[m2], 2.576[p1,p2], 3.894[p3], 3.564[p4]

Experimental data: [a*]Ref. [4], [b*]ref. [7], [c*]ref. [6], [d*]ref. [5], [e*]ref. [23], [f*]ref. [20], [g*]ref. [2].
Previous theoretical data: [a]Ref. [19], [b]ref. [23], [c]ref. [8], [d]ref. [19], [e]ref. [24], [f1]ref. [20]⇒LDA, [f2]ref. [20] ⇒GGA, [g]Ref. [22], [h]ref. [21], [h1]ref. [21] = > LDA, [h2]ref. [21] = > GGA, [i]ref. [12], [j]ref. [13], [k]ref. [15], [l1]ref. [14] = > LDA, [l2]ref. [14] = > GGA, [m]ref. [17], [m1]ref. [17] = > GGA, [m2]ref. [17] = > mBJ, [n]ref. [10], [o1]ref. [11] = > LDA, [o2]ref. [11] = > GGA, [p1]ref. [3] = > LDA, [p2]ref. [3] = > GGA, [p3]ref. [3] = > LDA + mBJ, [p4]ref. [3] = > GGA + mBJ.

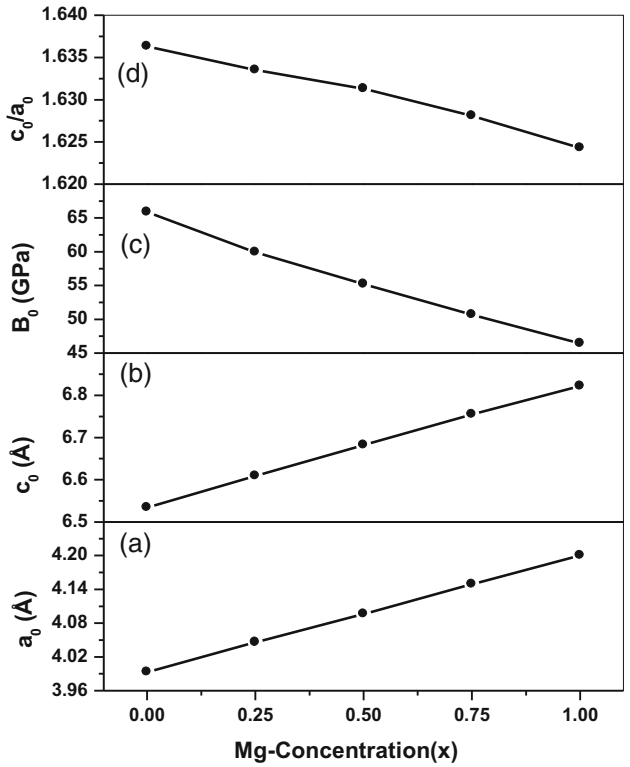

Figure 1. Mg-concentration dependence curve of the calculated (**a**) a_0, (**b**) c_0, (**c**) B_0 and (**d**) c_0/a_0 for the specimens under the w-$Mg_xZn_{1-x}Se$ system.

cell from the relation $V_0 = \sqrt{3}a_0^2c_0/2$. Computed optimised $a_0, c_0, c/a$ ratio, u and B_0 values for all binary and ternary specimens are presented in table 1. The computed structural data for binary w-ZnSe and w-MgSe show good accordance with the corresponding available experimental data for w-ZnSe [4–7,23] and w-MgSe [2] as well as some earlier theoretical data (see table 1). The structural data for the ternary alloys from any experiment or earlier calculation have not yet been reported in the literature.

The relation $\Delta c_0/a_0 = c_0/a_0 - 1.633$ determines the stability of any crystal structure in either the zinc-blende or the wurtzite phase [9]. The positive value of $\Delta c_0/a_0$ indicates the stability of a crystal in the zinc-blend structure, while the negative value of $\Delta c_0/a_0$ confirms its stability in the wurtzite phase [9]. We have used our optimised c_0/a_0 values for the five specimens to check their respective phase stability. The calculated optimised value of c_0/a_0 for ZnSe and MgSe, extremely close to the corresponding experimental data [2,5], indicates positive and negative $\Delta c_0/a_0$ and hence ZnSe and MgSe are stable in zinc-blende and wurtzite phases, respectively. Computed optimised c_0/a_0 value provides positive $\Delta c_0/a_0$ for $Mg_{0.25}Zn_{0.75}Se$ ternary alloy. Hence, it is stable in the zinc-blende phase. In the case of $Mg_{0.50}Zn_{0.50}Se$ and $Mg_{0.75}Zn_{0.25}Se$ ternary alloys, the computed optimised c_0/a_0 value provides negative $\Delta c_0/a_0$, and each of them shows stability in the wurtzite structure.

Nonlinear variations of a_0, c_0, B_0 and c_0/a_0 at different Mg-compositions (x) in the $Mg_xZn_{1-x}Se$ ternary system are shown in figures 1a–1d, respectively. Each calculated value of a_0 and c_0 enhances almost linearly as magnesium composition (x) enhances in the system. Such compositional variations of a_0 and c_0 show marginally slight upward deviation from the corresponding linear variation [33] in figures 1a and 1b, respectively. It is due to the successive substitution of pair(s) of smaller Zn atoms (radius = 1.42 Å) with slightly larger Mg atoms (radius = 1.45 Å). The nature of the $B_0(x)$ curve of this system in figure 1c is opposite to its $a_0(x)$ and $c_0(x)$ curves because of the relation $B \propto V^{-1}$. It also shows a slight downward deviation from the corresponding linear variation. It is to be noted from figure 1d that the computed c_0/a_0 value reduces nonlinearly as x enhances in the system. The following quadratic equations represent nonlinearity in $a_0(x)$, $c_0(x)$ and $B_0(x)$ curves of the w-$Mg_xZn_{1-x}Se$ system.

$$a_0(x) = 3.993 + 0.208x - 0.001x^2 \text{ (in Å unit)} \quad (1)$$

$$c_0(x) = 6.534 + 0.307x - 0.018x^2 \text{ (in Å unit)} \quad (2)$$

$$B_0(x) = 65.76 - 3.39x + 4.150x^2 \text{ (in GPa unit)} \quad (3)$$

From eqs (1) and (2), the calculated marginally small upward lattice constant bowing parameter in the $a_0(x)$ and $c_0(x)$ curve is −0.001 Å and −0.018 Å, respectively. On the other hand, eq. (3) shows that the calculated downward bulk modulus bowing parameter in the $B_0(x)$ curve is 4.15 GPa.

3.2 *Electronic properties*

With the aid of first-principle calculations in association with mBJ-GGA potentials, we have explored the electronic properties of the wurtzite specimens under the $Mg_xZn_{1-x}Se$ system, which would help identify their area of optoelectronic applications. Figures SF2a–e in the Supplementary Materials present the calculated band structure of $Mg_xZn_{1-x}Se$ alloys when $x = 0.0$, 0.25, 0.50, 0.75 and 1.0, respectively. Any wurtzite specimen under the $Mg_xZn_{1-x}Se$ system possesses a direct band gap. It is due to the existence of conduction band minima (CBM) and valence band maxima (VBM) on the same symmetry position (Γ–Γ) in the respective band structure. Hence, the transition from VBM to the CBM leaves the momentum of electrons unaltered.

We have analysed the origin of electronic states in diverse energy regions of the band structure of each

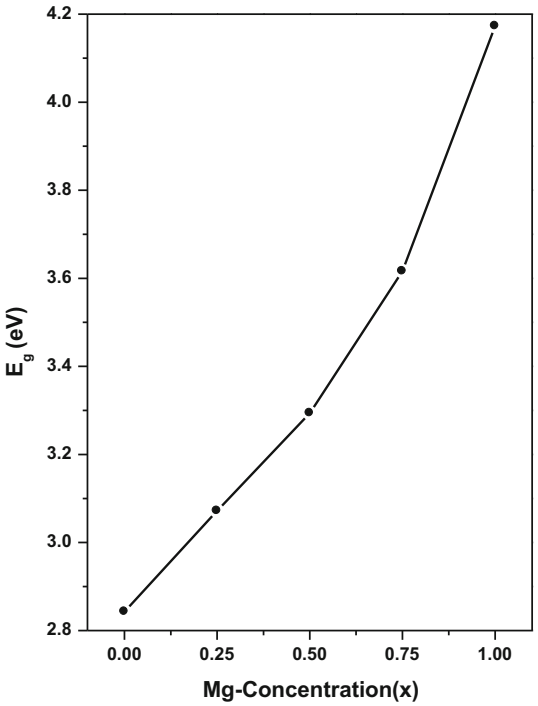

Figure 2. Mg-concentration dependence curve of the calculated minimum band-gap energy (E_g) for the specimens under the w-$Mg_xZn_{1-x}Se$ system.

specimen under the $Mg_xZn_{1-x}Se$ system from the calculations of the respective total density of states (TDOS) of the specimens and the constituent atoms along with the partial density of states (PDOS) of the constituent atoms. Figures SF3a–e of the Supplementary Materials show the calculated TDOS of wurtzite ZnSe, $Mg_{0.25}Zn_{0.75}Se$, $Mg_{0.50}Zn_{0.50}Se$, $Mg_{0.75}Zn_{0.25}Se$ and MgSe (filled grey curves), respectively, and their constituent atoms (line curves) are presented. The Fermi level in any band structure is taken at 0.0 eV. Closest to the Fermi level, the electronic states in the valence band region of the band structure of all the binary and ternary specimens come mainly from the 4p orbital of the selenium atom. Closest to the Fermi level, the electronic states in the conduction band region of w-ZnSe are dominantly contributed by the 4s orbital of the Zn atom. In contrast, w-MgSe is dominantly contributed by the 3p orbital of the Mg atom. The collective contribution of Zn-4s and Mg-3p orbitals significantly helps to form the electronic states in the conduction band region of the band structure of the ternary alloys near the Fermi level.

Table 1 also contains the fundamental band-gap energy (E_g) of the wurtzite specimens under the $Mg_xZn_{1-x}Se$ system. The calculated E_g of w-ZnSe is very close to the corresponding experimental [5] and the previously estimated [20] data. Any experimentally measured E_g for w-MgSe have not yet been reported, but our calculated data are similar to the earlier computed data [17]. Because of the non-availability of any experimental or earlier computed E_g in literature, verifying the same for any considered ternary specimen is impossible.

The nonlinear increase in the computed E_g with increasing x in the w-$Mg_xZn_{1-x}Se$ ternary system is shown in figure 2 and the curve shows a fair downward deviation from the corresponding linear variation. The electronegativities of the Zn, Mg and Se atoms are 1.65, 1.31 and 2.55, respectively. Therefore, the electronegativity difference between the Zn and Se atoms in the initial binary compound w-ZnSe is smaller than that between Mg and Se atoms in the terminal binary compound w-MgSe. As we proceed from w-ZnSe to w-MgSe via the formation of ternary alloys through gradual substitution of Zn with Mg atom(s), the gradual increase in the resultant electronegativity difference increases the ionic character and hence decreases the orbital overlap, which ultimately increases the band gap. The following quadratic equation represents the nonlinearity in $E_g(x)$ curve of the system.

$$E_g(x) = 2.867 + 0.418x + 0.864x^2 \text{ (in eV unit)}. \quad (4)$$

The downward bowing parameter in the $E_g(x)$ curve of the w-$Mg_xZn_{1-x}Se$ system is 0.864 eV. The fair electronegativity difference between the dissimilar atoms, zinc (1.65) and magnesium (1.31), in the terminal binary w-ZnSe and w-MgSe of the system is responsible for such a fair amount of bowing.

3.3 *Optical properties*

The optical properties of any semiconductor specimen are useful in finding the area of its optoelectronic applications, and they are strongly dependent on the electronic properties of the said semiconductor. For a material, the optical characteristics are analysed by calculating the energy/frequency spectrum of the real part $\varepsilon_1(\omega)$ and imaginary part $\varepsilon_2(\omega)$ of the frequency-dependent dielectric function $\varepsilon(\omega)$. They are related to the dispersion and absorption of the incident energy by the specimen, respectively. $\varepsilon(\omega)$ is expressed as [34]

$$\varepsilon(\omega) = \varepsilon_1(\omega) + \varepsilon_2(\omega). \quad (5)$$

Integrating over the first Brillouin zone, we get $\varepsilon_2(\omega)$ of any material as [35]

$$\varepsilon_2(\omega) = \frac{8\pi^2 e^2}{\omega^2 m^2} \sum_n \sum_{n'} \int_{BZ} \left| P^v_{nn'}(k) \right|^2 f_{kn}(1 - f_{kn'}) \times \partial(E^k_n - E^k_{n'} - \hbar\omega) \frac{\partial^3 k}{2\pi^3}. \quad (6)$$

The following Kramer–Kronig transformation expresses $\varepsilon_1(\omega)$ in terms of $\varepsilon_2(\omega)$ [35]:

$$\varepsilon_1(\omega) = 1 + \frac{2}{\pi} P \int_0^\infty \frac{\omega' \varepsilon_2(\omega')}{\omega'^2 - \omega^2} \mathrm{d}\omega' \tag{7}$$

In terms of $\varepsilon_1(\omega)$ and $\varepsilon_2(\omega)$, the refractive index $n(\omega)$, extinction coefficient $k(\omega)$, normal incidence reflectivity $R(\omega)$, optical conductivity $\sigma(\omega)$, optical absorption coefficient $\alpha(\omega)$, energy loss function $L(\omega)$ and transmission coefficient $T(\omega)$ of a material can be calculated using the following expressions [34–36].

The complex refractive index is $\tilde{n}(\omega) = n(\omega) + ik(\omega)$ [34]. The following Kramer–Kronig transformations connect the real part $n(\omega)$ and the imaginary part $k(\omega)$ as [36]

$$n(\omega) = 1 + \frac{2}{\pi} P \int_0^\infty \frac{k(\omega')}{\omega' - \omega} \mathrm{d}\omega' \tag{8}$$

$$k(\omega) = -\frac{2P}{\pi} \int_0^\infty \frac{n(\omega') - 1}{\omega' - \omega} \mathrm{d}\omega'. \tag{9}$$

The frequency-dependent $n(\omega)$ and $k(\omega)$ are calculated using the following relations [35]:

$$n(\omega) = \left[\frac{\sqrt{\varepsilon_1^2(\omega) + \varepsilon_2^2(\omega)}}{2} + \frac{\varepsilon_1(\omega)}{2} \right]^{1/2} \tag{10}$$

$$k(\omega) = \left[\frac{\sqrt{\varepsilon_1^2(\omega) + \varepsilon_2^2(\omega)}}{2} - \frac{\varepsilon_1(\omega)}{2} \right]^{1/2}. \tag{11}$$

The frequency-dependent normal incidence reflectivity $R(\omega)$ of a material is [35]

$$R(\omega) = \frac{(1-n)^2 + k^2}{(1+n)^2 + k^2}. \tag{12}$$

The optical conductivity as a function of frequency, i.e. $\sigma(\omega)$, is [34]

$$\sigma(\omega) = \frac{2 W_{ev} \hbar \omega}{|\vec{E}_0|}. \tag{13}$$

The optical absorption coefficient as a function of frequency, i.e. $\alpha(\omega)$, is [35]

$$\alpha(\omega) = \sqrt{2\omega} \left[\sqrt{\varepsilon_1^2(\omega) + \varepsilon_2^2(\omega)} - \varepsilon_1(\omega) \right]^{\frac{1}{2}}. \tag{14}$$

The frequency-dependent energy loss function $L(\omega)$ of the electrons of a material [35] is

$$L(\omega) = -\mathrm{Im}\left(\frac{1}{\varepsilon}\right) = \frac{\varepsilon_2(\omega)}{\varepsilon_1^2(\omega) + \varepsilon_2^2(\omega)}. \tag{15}$$

The frequency-dependent transmission coefficient $T(\omega)$ of a material is connected to the corresponding absorption coefficient $\alpha(\omega)$ through the relation [34]

$$\alpha(\omega) = 2.303 \ln\left(\frac{1}{T(\omega)}\right). \tag{16}$$

Any optical parameter $M(\omega)$ is bifurcated into ordinary component $M^{xx}(\omega)$ and extraordinary component $M^{zz}(\omega)$ due to the hexagonal symmetry of the crystal. They indicate that the electromagnetic radiation, interacting with the specimen, is polarised perpendicular to the c-axis, i.e. along the x-axis and parallel to c-axis, i.e. along the z-axis, respectively. The computed frequency response spectrum of xx and zz components of $\varepsilon_1(\omega)$ of the wurtzite ZnSe, $Mg_{0.25}Zn_{0.75}Se$, $Mg_{0.50}Zn_{0.50}Se$, $Mg_{0.75}Zn_{0.25}Se$ and MgSe in the incident energy range 0.0–30.0 eV are presented as figures 3a–3e, respectively, while the same of $\varepsilon_2(\omega)$ for these specimens are shown in figures 4a–4e, respectively. On the other hand, figures SF4–SF10a–e in the Supplementary Materials present the frequency spectrum of both the components of $n(\omega)$, $k(\omega)$, $R(\omega)$, $\sigma(\omega)$, $\alpha(\omega)$, $L(\omega)$ and $T(\omega)$ of these specimens, respectively in the incident energy range 0.0–30.0 eV. Moreover, components of various optical constants for all the wurtzite specimens under consideration are calculated and presented in this paper. From the frequency response curves, we have seen that each

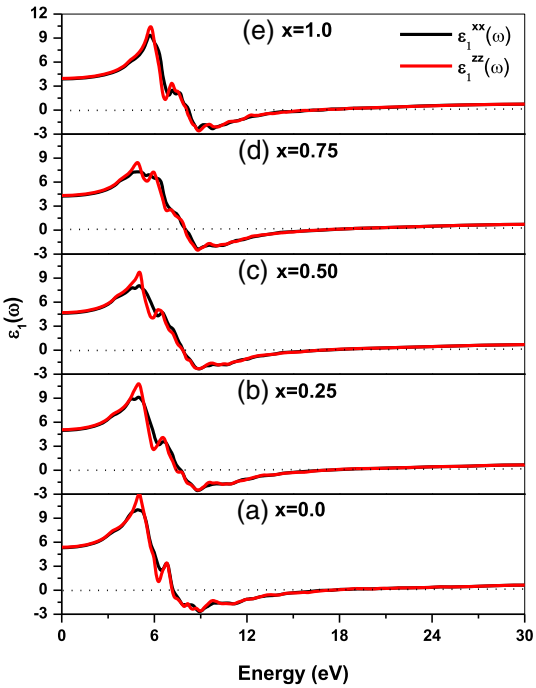

Figure 3. Variation of $\varepsilon_1^{xx}(\omega)$ and $\varepsilon_1^{zz}(\omega)$ components of $\varepsilon_1(\omega)$ for the specimens under the w-$Mg_xZn_{1-x}Se$ ternary system as a function of incident energy when (**a**) $x = 0.0$, (**b**) $x = 0.25$, (**c**) $x = 0.50$, (**d**) $x = 0.75$ and (**e**) $x = 1.0$.

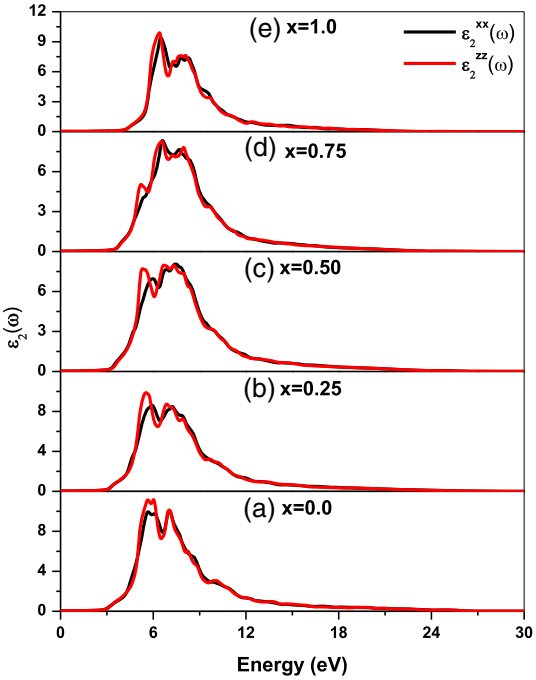

Figure 4. Variation of $\varepsilon_2^{xx}(\omega)$ and $\varepsilon_2^{zz}(\omega)$ components of $\varepsilon_2(\omega)$ for the specimens under the w-$Mg_xZn_{1-x}Se$ ternary system as a function of incident energy when (**a**) $x = 0.0$, (**b**) $x = 0.25$, (**c**) $x = 0.50$, (**d**) $x = 0.75$ and (**e**) $x = 1.0$.

of these optical parameters shows anisotropy [$M^{xx}(\omega) \neq M^{zz}(\omega)$] in the small energy range around the respective peak region. At the same time, they are almost isotropic in the preceding and subsequent energy regions.

3.3.1 *Frequency dependence of different optical parameters.* The peaks in $\varepsilon_1^{xx}(\omega)$ and $\varepsilon_1^{zz}(\omega)$ spectra within the UV region below 7.0 eV indicate prominent dispersion of incident radiation by the specimens considered in figures 3a–3e. On the other hand, prominent absorption of incident radiation by the considered specimens is indicated by the presence of peaks in $\varepsilon_2^{xx}(\omega)$ and $\varepsilon_2^{zz}(\omega)$ spectrum within the UV region 5.0–11.0 eV in figures 4a–4e. Each specimen shows metallic character due to the negative $\varepsilon_1^{xx}(\omega)$ and $\varepsilon_1^{zz}(\omega)$ within the 8.0–15.0 eV energy region. Beyond 15.0 eV, our specimens show marginally positive $\varepsilon_1^{xx}(\omega)$ and $\varepsilon_1^{zz}(\omega)$ values. The peaks in the $\varepsilon_2^{xx}(\omega)$ and $\varepsilon_2^{zz}(\omega)$ spectra of these specimens are originated from the exclusive or collective effort of electronic excitations from the occupied Se-4p state of the valence band to the unoccupied Zn-4s and Mg-3p states of the conduction band.

In figures SF4a–e, both the $n^{xx}(\omega)$ and $n^{zz}(\omega)$ components of $n(\omega)$ for each specimen show peaks and hence maximum refractive index $n(\omega)_{max}$ in the UV region below 8.0 eV of incident energy. On the other hand, each component becomes lower than unity ($c/v < 1$) above 9.5 eV. It is a signature of the opacity of each material and it ensures a smaller free-space light velocity (c) than the group velocity ($v_g = c/n$) of propagation of wave packets through these materials [37].

Uniaxial birefringence results from the optical anisotropy in a crystal, which shows the dependence of the refractive index on the direction of the applied electric field in a material. The birefringence results in double refraction in the crystal and hence refractive index is bifurcated into the extraordinary component n_e (zz-component) and ordinary component n_o (xx-component). $\Delta n = n_e – n_o$ at some frequency/wavelength is the measurement of the birefringence of a material [38]. The positive uniaxial crystal is indicated with $n_e > n_o$, while $n_e < n_o$ is the signature of the negative uniaxial crystal. Figure 5 shows the birefringence of our wurtzite specimens. Positive birefringence is shown by each specimen up to about 5.0 eV and hence the speed of the ordinary rays is much higher. Dispersion is lower than the extraordinary rays in this energy range. Simultaneous positive and negative birefringence with a negative value slightly higher than positive is observed in the subsequent energy region up to about 18.0 eV. It is the signature of a slightly higher speed but a lower dispersion of extraordinary rays than those of the ordinary rays in this segment of energy. The birefringence has important applications in liquid crystal displays, electronic cameras, light modulators, colour filters etc. [38].

Significantly high $k(\omega)$ with peaks is observed in the frequency spectrum of $k^{xx}(\omega)$ and $k^{zz}(\omega)$ components of

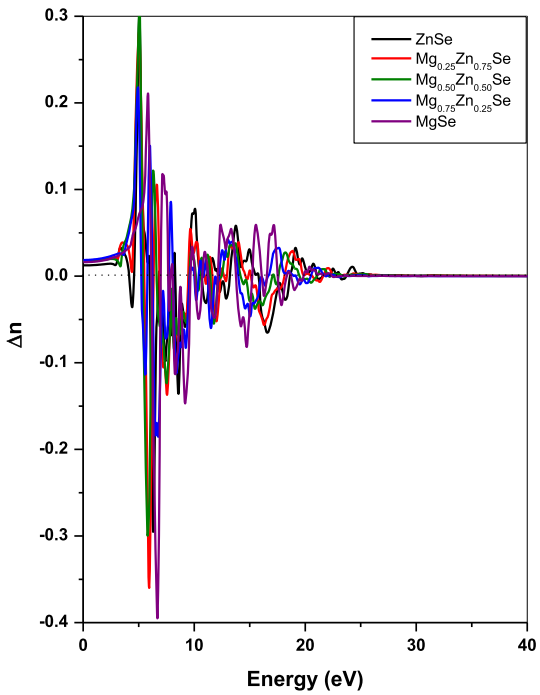

Figure 5. Birefringence of the wurtzite specimens under the $Mg_xZn_{1-x}Se$ system.

$k(\omega)$ in the 6.0–12.0 eV energy region, i.e. within the UV region in figures SF5a–e. It means that photons having 6.0–12.0 eV energy face much higher resistance during their travel through these semiconductor specimens than the photons having energy in the preceding and subsequent energy regions [37]. Figures SF6a–e show significantly high value (> 0.20) of both the components $R^{xx}(\omega)$ and $R^{zz}(\omega)$ of normal incidence reflectivity $R(\omega)$ of the considered specimens in the broad energy region 5.0–17.0 eV in their respective spectra. Each hexagonal specimen shows a significantly high (> 2000 $(\Omega^{-1}\cdot\text{cm}^{-1})$ value of both the components $\sigma^{xx}(\omega)$ and $\sigma^{zz}(\omega)$ of optical conductivity $\sigma(\omega)$ in the energy region 5.0–11.0 eV in figures SF7a–e. On the other hand, both the components $\alpha^{xx}(\omega)$ and $\alpha^{zz}(\omega)$ of the optical absorption coefficient $\alpha(\omega)$ show significantly high absorption of incident radiation (>100 cm^{-1}) in the 6.0–14.0 eV energy region in figures SF8a–e.

The energy loss of electrons due to their inelastic scattering with atoms in the crystal lattice of a material is investigated using the energy loss function $L(\omega)$. The nature of frequency response of any component of $L(\omega)$ of a specimen is opposite to the corresponding component of $\varepsilon_2(\omega)$. Each specimen shows a negligibly small value of components $L^{xx}(\omega)$ and $L^{zz}(\omega)$ of $L(\omega)$ in figures SF9a–e up to about 12.0 eV. On the other hand, both the components of $L(\omega)$ of each specimen show sufficiently high value and hence significant energy loss in the broad energy region 13.0–21.0 eV. The frequency at which the most intense peak occurs in the $L(\omega)$ spectrum of a material is known as the plasma resonance frequency of the material.

When incident energy is zero, a significantly high value of components $T^{xx}(\omega)$ and $T^{zz}(\omega)$ of transmission coefficient $T(\omega)$ (= 0.999) of any specimen is observed in figures SF10a–e. In each specimen, $T(\omega)$ is almost isotropic, i.e. $T^{xx}(\omega) \approx T^{zz}(\omega)$ up to 2.5 eV of incident energy, while the components of $T(\omega)$ show anisotropy beyond that energy. With the increase in energy, the components of $T(\omega)$ of all the specimens gradually decrease and finally it becomes almost zero at 4.98, 4.52, 4.36, 4.22 and 4.05 eV in the case of ZnSe, $Mg_{0.25}Zn_{0.75}Se$, $Mg_{0.50}Zn_{0.50}Se$, $Mg_{0.75}Zn_{0.25}Se$ and MgSe, respectively known as cut-off energy. It is to be noted that $E_{\text{cut-off}}$ exhibits red-shift with increasing x in the system.

3.3.2 *Optical constants.* The components of static dielectric constant $\varepsilon_1^{xx}(0)$ and $\varepsilon_1^{zz}(0)$, static refractive index $n^{xx}(0)$ and $n^{zz}(0)$ and static reflectivity $R^{xx}(0)$ and $R^{zz}(0)$ for each specimen are calculated from the corresponding spectra at almost zero frequency. Each of them is strongly dependent on the band gap of the material. The variation of $\varepsilon_1(0)$ of any semiconductor with its band gap is presented with the following equation as per the Penn model [39]:

$$\varepsilon_1(0) \approx 1 + \left(\frac{\hbar\omega_p}{E_g}\right)^2. \tag{17}$$

Moreover, since the relation between $n(0)$ and $\varepsilon_1(0)$ is $n(0) \approx \sqrt{\varepsilon_1(0)}$ and that between $R(0)$ and $n(0)$ is $R(0) = [\{1 - n(0)\}/\{1 + n(0)\}]^2$, the variation of $n(0)$ and $R(0)$ of any semiconductor with its band gap are presented as follows:

$$n(0) \approx \sqrt{1 + \left(\frac{\hbar\omega_p}{E_g}\right)^2}. \tag{18}$$

$$R(0) = \left[\frac{1 - \sqrt{1 + \left(\frac{\hbar\omega_p}{E_g}\right)^2}}{1 + \sqrt{1 + \left(\frac{\hbar\omega_p}{E_g}\right)^2}}\right]^2. \tag{19}$$

Equations (17)–(19) indicate that larger band-gap energy (E_g) semiconductor exhibits lower value of components of static optical constants $\varepsilon_1(0)$, $n(0)$ and $R(0)$ and vice versa. In table 2, we have observed that the calculated components of static optical constants $\varepsilon_1(0)$, $n(0)$ and $R(0)$ of the specimens under the w-Mg_xZn_{1-x}Se system reduce with the increase in x. On the other hand, table 1 and figure 2 show that the calculated E_g of the specimens under the same system increases with the increase in x. Such observations are well supported by eqs (17)–(19). The variations of xx and zz components of $\varepsilon_1(0)$, $n(0)$ and $R(0)$ with x in this system are presented in figures 6a–6c, respectively. Computed components of $\varepsilon_1(0)$ for w-MgSe are smaller than the corresponding components of $\varepsilon_1(0)$ calculated earlier [10]. Experimentally investigated or earlier calculated static optical constant of the other specimens is not yet reported in the literature, and hence we cannot verify their calculated static optical constant data.

Some empirical relationships exist [40–42], which relate refractive index at extremely low frequency $n(0)$ with minimum E_g of a semiconductor. Moss [40] proposed the empirical relation as

$$E_g n^4 = k. \tag{20}$$

Ravindra *et al* [41] have proposed the value of k = 108 eV. They have also offered another empirical relationship between $n(0)$ and E_g as

$$n = \alpha + \beta E_g. \tag{21}$$

The proposed values of α and β are 4.084 and $-0.62\ \text{eV}^{-1}$, respectively.

Table 2. Calculated components of zero-frequency limits $\varepsilon_1(0)$, $n(0)$ and $R(0)$.

Compounds	Components of zero-frequency limits											
	Static dielectric constant $\varepsilon_1(0)$		Static refractive index $n(0)$									
			FP-LAPW		Moss formula (eq. (20))		Rabindra formula (eq. (21))		Herve formula (eq. (22))		Static reflectivity $R(0)$	
	$\varepsilon_1^{xx}(0)$	$\varepsilon_1^{zz}(0)$	$n^{xx}(0)$	$n^{zz}(0)$	$n^{xx}(0)$	$n^{zz}(0)$	$n^{xx}(0)$	$n^{zz}(0)$	$n^{xx}(0)$	$n^{zz}(0)$	$R^{xx}(0)$	$R^{zz}(0)$
ZnSe	5.32	5.38	2.31	2.32	2.48	2.49	2.32	2.34	2.39	2.42	0.156	0.158
$Mg_{0.25}Zn_{0.75}Se$	4.98	5.06	2.23	2.25	2.43	2.45	2.18	2.22	2.33	2.34	0.145	0.148
$Mg_{0.50}Zn_{0.50}Se$	4.62	4.69	2.15	2.17	2.39	2.40	2.04	2.06	2.26	2.28	0.133	0.136
$Mg_{0.75}Zn_{0.25}Se$	4.26	4.33	2.06	2.08	2.34	2.36	1.84	1.87	2.18	2.19	0.120	0.123
MgSe	3.90 4.94[a]	3.96 4.82[a]	1.97	1.99	2.25	2.27	1.49	1.53	2.05	2.07	0.107	0.110

Previous theoretical data: [a]Ref. [10]

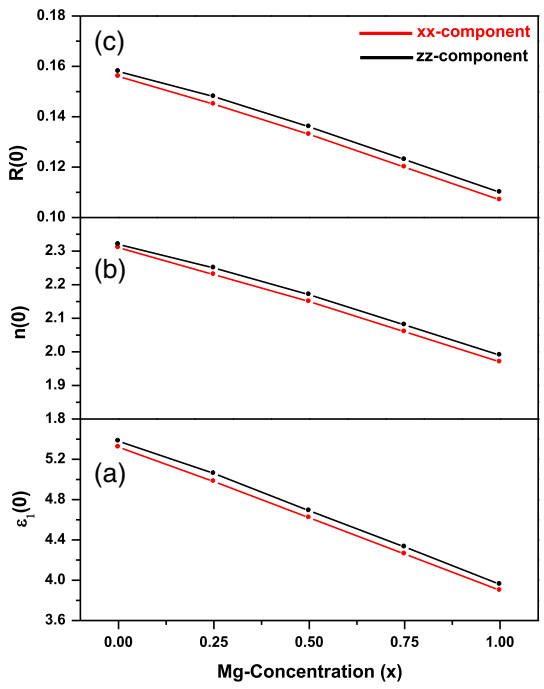

Figure 6. Variation of *xx* and *zz* components of the computed (**a**) $\varepsilon_1(0)$, (**b**) $n(0)$, (**c**) $R(0)$ as a function of x for the wurtzite specimens under the $Mg_xZn_{1-x}Se$ system.

Herve and Vandamme [42] proposed another empirical relation as

$$n = \sqrt{1 + \left(\frac{A}{E_g + B}\right)^2}. \tag{22}$$

Here, the proposed values of A and B are 13.6 eV and 3.4 eV, respectively.

Variation of components of refractive index at extremely low frequency, i.e. $n^{xx}(0)$ and $n^{zz}(0)$ with E_g of the specimens under the w-$Mg_xZn_{1-x}Se$ system have been examined again with eqs (20)–(22). $n^{xx}(0)$ and $n^{zz}(0)$ for all the specimens, calculated using eqs (20)–(22), are also reported in table 2. Tables 1 and 2 show that the lower band-gap semiconductors possess larger values of $n^{xx}(0)$ and $n^{zz}(0)$ and vice versa. It is also observed from table 2 that the FP-LAPW-based calculated $n^{xx}(0)$ and $n^{zz}(0)$ of each considered specimen are in good accordance with the corresponding components of $n(0)$ calculated using eqs (20)–(22).

The minimum amount of incident energy at which components of $\varepsilon_2(\omega)$, $k(\omega)$, $\sigma(\omega)$ and $\alpha(\omega)$ start interacting with incident radiation is called the critical point energy (E_c) in the corresponding frequency response spectrum. The computed E_c for all the considered specimens are reported in table 3, and each shows strong band-gap dependence. With increasing x in the w-$Mg_xZn_{1-x}Se$ system, the calculated E_c in the spectrum of both the components of $\varepsilon_2(\omega)$, $k(\omega)$, $\sigma(\omega)$, $\alpha(\omega)$ of the considered specimens in table 3 and E_g of the specimens in table 1 increase.

Table 3. Calculated critical points (eV) in the spectra of the components of $\varepsilon_2(\omega)$, $k(\omega)$, $\sigma(\omega)$, $\alpha(\omega)$.

	Critical points (eV) in the spectra of							
Compounds	$\varepsilon_2^{xx}(\omega)$	$\varepsilon_2^{zz}(\omega)$	$k^{xx}(\omega)$	$k^{zz}(\omega)$	$\sigma^{xx}(\omega)$	$\sigma^{zz}(\omega)$	$\alpha^{xx}(\omega)$	$\alpha^{zz}(\omega)$
ZnSe	2.825	2.857	2.828	2.874	2.790	2.804	2.857	2.871
$Mg_{0.25}Zn_{0.75}Se$	3.056	3.083	2.933	2.951	3.048	3.076	3.079	3.106
$Mg_{0.50}Zn_{0.50}Se$	3.231	3.288	3.130	3.179	3.250	3.308	3.270	3.325
$Mg_{0.75}Zn_{0.25}Se$	3.514	3.525	3.541	3.569	3.586	3.608	3.563	3.582
MgSe	4.192	4.195	4.170	4.173	4.152	4.158	4.162	4.171

4. Conclusion

Density functional theory-oriented FP-LAPW calculations explore structural, electronic and optical characteristics of wurtzite specimens constituting the $Mg_xZn_{1-x}Se$ system. Almost linear enhancement in lattice constants (a_0, c_0), while a nonlinear reduction in c_0/a_0 and bulk modulus (B_0) are observed with increasing x. ZnSe and MgSe are stable in the zinc-blende (B3) and wurtzite (B4) structure, respectively. On the other hand, though the $Mg_{0.25}Zn_{0.75}Se$ ternary alloy is stable in the zinc-blende phase, the other two, i.e. $Mg_{0.50}Zn_{0.50}Se$ and $Mg_{0.75}Zn_{0.25}Se$ ternary alloys are stable in the wurtzite structure. Calculations show the direct band-gap ($\Gamma-\Gamma$) semiconductor character of each wurtzite specimen under consideration. The composition (x) dependence curve of the minimum band gap shows non-linear enhancement with increasing x. Each optical parameter of the considered wurtzite specimens shows optical anisotropy resulting from hexagonal symmetry. Hence, each is bifurcated into xx (ordinary) and zz (extraordinary) components. The calculated ordinary (n_o) and extraordinary (n_e) components of the refractive index of each wurtzite specimen exhibit uniaxial birefringence. Electronic transitions from Se-4p level of the valence region to Zn-4s and Mg-3p levels of the conduction region of the band structure near the Fermi level significantly contribute to the diverse optical phenomena in the UV region. It confirms their compatibility in fabricating various UV optoelectronic devices. The calculated Mg-concentration dependence curves of xx and zz components of static optical constants $\varepsilon_1(0)$, $n(0)$, $R(0)$ of the specimens show opposite behaviour. At the same time, the critical point energy in each of the $\varepsilon_2(\omega)$, $k(\omega)$, $\sigma(\omega)$, $\alpha(\omega)$ spectra exhibits a nature identical to the corresponding concentration dependence curve of the fundamental band gap of the system.

References

[1] O Medelung (Ed.), *Landolt Bornstein: Numerical data and functional relationship in science and technology* (Springer, Berlin, 1982) Vol. 17b
[2] V H Mittendorf, *Z. Phys.* **183**, 113 (1965)
[3] H Elsayed, D Olguın, A Cantarero and I Hernandez-Calderon, *Phys. Status Solidi B* **252**, 663 (2015)
[4] W M Yim and E J Stofko, *J. Electrochem. Soc.* **119**, 381 (1972)
[5] Y S Park and F L Chan, *J. Appl. Phys.* **36**, 800 (1965)
[6] X Zhang, D Wang, M Beres, L Liu, Z Ma, P Y Yu and S S Mao, *Appl. Phys. Lett.* **103**, 082111 (2013)
[7] H I Wang, W T Tang, L W Liao, P S Tseng, C W Luo, C S Yang and T K Kobayashi, *J. Nanomater.* **2012**, 1 (2012)
[8] L V Atroshchenko, E F Voronkin, S N Galkin, A I Lalayants, I A Rybalka, V D Ryzhikov and A G Fedorov, *Inorg. Mater.* **40**, 563 (2004)
[9] P Lawaetz, *Phys. Rev. B* **5**, 4039 (1972)
[10] S Duman, S Bagci, H M Tutuncu and G P Srivastava, *Phys. Rev. B* **73**, 205201 (2006)
[11] G Gokoglu, M Durandurdu and O Gulseren, *Comput. Mater. Sci.* **47**, 593 (2009)
[12] P E Van Camp and V E Van Doren, *Phys. Rev. B* **55**, 775 (1997)
[13] R Pandey and A Sutjianto, *Solid State Commun.* **91**, 269 (1994)
[14] D Rached, N Benkhettou, B Soudini, B Abbar, N Sekkal and M Driz, *Phys. Status Solidi B* **240**, 565 (2003)
[15] A Chakrabarti, *Phys. Rev. B* **62**, 1806 (2000)
[16] S H Mir, P C Jha, S Dabhi and P K Jha, *Mater. Chem. Phys.* **175**, 54 (2016)
[17] L Tairi, S Touam, A Boumaza, M Boukhtouta, H Meradji, S Ghemid, S Bin Omran, F El Haj Hassan and R Khenata, *Phase Transit.* **90**, 929 (2017)
[18] S G Lee and K J Chang, *Phys. Rev. B* **52**, 1918 (1995)
[19] C Y Yeh, Z W Lu, S Froyen and A Zunger, *Phys. Rev. B* **46**, 10086 (1992)
[20] O Zakharov, A Rubio, X Blase, M L Cohen and S G Louie, *Phys. Rev. B* **50**, 10780 (1994)

[21] S Zh Karazhanov, P Ravindran, A Kjekshus, H Fjellvag, U Grossner and B G Svensson, *J. Appl. Phys.* **100**, 043709 (2006)
[22] I Khan, I Ahmad, H A R Aliabad and M Maqbool, arXiv: 1201.0870 [cond-mat.str-el] (2012)
[23] S Zh Karazhanov, P Ravindran, A Kjekshus H Fjellvag and B G Svensson, arXiv:0705.2550v1 [cond-mat.soft] (2007)
[24] H Momida and T Oguchi, *Appl. Phys. Exp.* **11**, 041201 (2018)
[25] P Hohenberg and W Kohn, *Phys. Rev.* **136**, B864 (1964)
[26] W Kohn and L J Sham, *Phys. Rev.* **140**, A1133 (1965)
[27] O K Andersen, *Phys. Rev. B* **42**, 3063 (1975)
[28] P Blaha, K Schwarz, G H Madsen, D Kbasnicka and J Luitz, *FP-LAPW+lo program for calculating crystal properties* edited by K Schwarz (Techn. WIEN2K, Austria, 2001)
[29] Z Wu and E R Cohen, *Phys. Rev. B* **73**, 235116 (2006)
[30] F Tran and P Blaha, *Phys. Rev. Lett.* **102**, 226401 (2009)
[31] A Kokalj, *Comput. Mater. Sci.* **28**, 155 (2003)
[32] F D Murnaghan, *Proc. Natl. Acad. Sci. USA* **30**, 244 (1944)
[33] L Vegard, *Z. Phys.* **5**, 17 (1921)
[34] G Murtaza, I Ahmad, B Amin, A Afaq, F Ghafoor and A Benamrani, *Physica B* **406**, 2632 (2011)
[35] F Ahmadian and A Salary, *J. Kor. Phys. Soc.* **68**, 227 (2016)
[36] N W Ashcroft and N D Mermin, *Solid state physics* (Harcourt Brace College Publishers, New York, 1976)
[37] M Fox, *Optical properties of solids* (Oxford University Press, UK, 2001)
[38] I Khan, I Ahmad, H A R Aliabad, S J Asadabadi, Z Ali and M Maqbool, *Comput. Mater. Sci.* **77**, 145 (2013)
[39] D R Penn, *Phys. Rev.* **128**, 2093 (1962)
[40] V P Gupta and N M Ravindra, *Phys. Status Solidi B* **10**, 715 (1980)
[41] N M Ravindra, S Auluck and V K Srivastava, *Phys. Status Solidi B* **93**, K155 (1979)
[42] J P L Herve and L K J Vandamme, *Infrared Phys. Technol.* **35**, 609 (1994)